Heliyon 10 (2024) e24238

Contents lists available at ScienceDirect

Heliyon

journal homepage: www.cell.com/heliyon

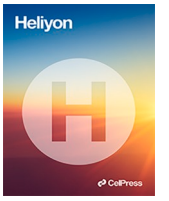

Research article

Characterization and treatment effects on Mutaka kaolin for additive in coatings: Mineral composition, thermal and structural modifications

Andrew Kasumba Buyondo [a,*], Hillary Kasedde [a], John Baptist Kirabira [a], Ocident Bongomin [b]

[a] Department of Mechanical Engineering, Makerere University Kampala, P. O. Box 7062, Kampala, Uganda
[b] Department of Manufacturing, Textiles and Industrial Engineering, School of Engineering, Moi University, P. O. Box 3900-30100, Eldoret, Kenya

ARTICLE INFO

Keywords:
Mutaka kaolin
Coatings
Additive
Crystallinity
And TiO_2

ABSTRACT

Previous studies in Uganda have primarily explored kaolin's applications in composites, pottery, bricks, and insulation, neglecting its potential for coatings and paints, which is crucial for industrialization and saving foreign exchange. This study investigates the transformation of kaolin through various treatments and analyzes their impacts on its physical and chemical properties for potential use in coating applications. Thermal analysis, X-ray Fluorescence Spectroscopy (XRF), X-ray diffraction (XRD), Fourier-transform infrared spectroscopy (FTIR), scanning electron microscopy with energy-dispersive X-ray spectroscopy (SEM-EDS), and transmission electron microscopy (TEM) techniques were employed to assess these alterations. The results show that thermal treatment of kaolin at 45.9 °C had minimal impact on mass loss, while the crystallinity of kaolinite was found to be lost around 600 °C, resulting in structural changes. XRF result demonstrates variations in SiO_2 and Al_2O_3 composition, with low TiO_2 content desirable for paint and coating applications. XRD results showed well-defined diffractions associated with kaolinite in all treated and untreated kaolin samples. The presence of K-feldspar and quartz are also identified. However, the thermal treatment at 800 °C transforms kaolinite into metakaolin, essential for enhancing coating properties. SEM-EDS results indicate increased porosity and reduced impurities in the thermal-treated sample, which might enhance the whiteness and suitability of pigment and binder dispersion in coatings. TEM images confirmed the hexagonal nature of kaolinite platelets and demonstrated the amorphous nature of kaolin nanoparticles with ammonium molybdate treatment, which led to the delamination and exfoliation of kaolinite layers, improving dispersibility. Kaolin thermally treated exhibited good crystallinity, solid growth, cubic morphology, and uniform size distribution. These findings suggest that tailored treatments can optimize kaolin's properties, making it a promising additive for high-performance coatings.

1. Introduction

The market growth of material coatings is fueled by increased construction activities worldwide and the growing urban population

* Corresponding author. Department of Mechanical Engineering, Makerere University Kampala, P. O. Box 7062, Kampala, Uganda.
E-mail addresses: kasumba.andrew89@students.mak.ac.ug, kasumba.andrew@gmail.com (A.K. Buyondo).

https://doi.org/10.1016/j.heliyon.2024.e24238
Received 5 September 2023; Received in revised form 11 October 2023; Accepted 4 January 2024
Available online 6 January 2024

[1]. These factors have emerged as significant drivers behind the rising demand for material coatings in various industries [2]. However, addressing the significant environmental burdens associated with building and construction materials is important. These burdens pose global concerns due to their adverse effects on air quality, human health, and contribution to climate change [3,4]. Among the building materials, paints and coatings produced from chemical-based pigments are identified as one of the major hazardous pollutants by the World Health Organization (WHO) [5], which could lead to different types of cancers [6,7]. Alkyd semi-gloss paint, alkyd resin, and titanium dioxide (TiO_2) are significant contributors to energy consumption and environmental emissions in chemical-based pigments. These factors contribute to the release of volatile organic compounds (VOCs), carbon dioxide (CO_2), sulfur dioxide (SO_2), nitrogen oxides (NOx), and chemical oxygen demand (COD) into the environment [2,8]. Apart from alkyd resin and TiO_2 pigments, oxygenated and hydrocarbon solvents pose significant environmental and human health hazards in coatings. When these solvents are used in poorly ventilated areas, their vapors can irritate the eyes, skin, and lungs. They can contribute to various health issues, including kidney damage, muscle weakness, respiratory problems, and liver disorders [2,4,8].

These challenges have led to different approaches to energy consumption management and bio-based materials such as pigment to increase efficiency and reduce environmental pollution, including greenhouse gas emissions [9–11]. One such positive alternative for chemical-based and mineral fillers is kaolinite, which may fill the demand gaps with significant reductions in the environmental impacts.

Kaolinite is a precious and versatile mineral widely utilized across various industries. This is primarily due to its unique physical and chemical properties, as well as its surface chemistry and crystal structure [12]. It is used extensively in the ceramics [13], refractory [14], rubber [2], fillers [15], cement [16], and pharmaceutical industries [17]. Kaolinite is a mineral found in numerous countries worldwide, although only a few deposits are of high quality. The classification of raw kaolinite into different grades typically influences its price and determines its suitability for specific industrial applications. These graded classifications help to differentiate the various qualities of kaolinite and guide its utilization in various industries. Among industrial applications, kaolinite minerals can be used as a pigment and extender in paint and coating formulations [18], often a less expensive alternative to TiO_2. These enhancements offer several benefits to paint, including reduced weight per container, significantly extended product lifespan, and improvements in opacity, gloss, color, and viscosity [19].

With increasing and new applications of kaolin resources, promising deposits are worth exploiting in any strategic location. In Uganda, kaolin deposits occur abundantly in different regions, yet detailed investigation of raw materials, characterization, phase

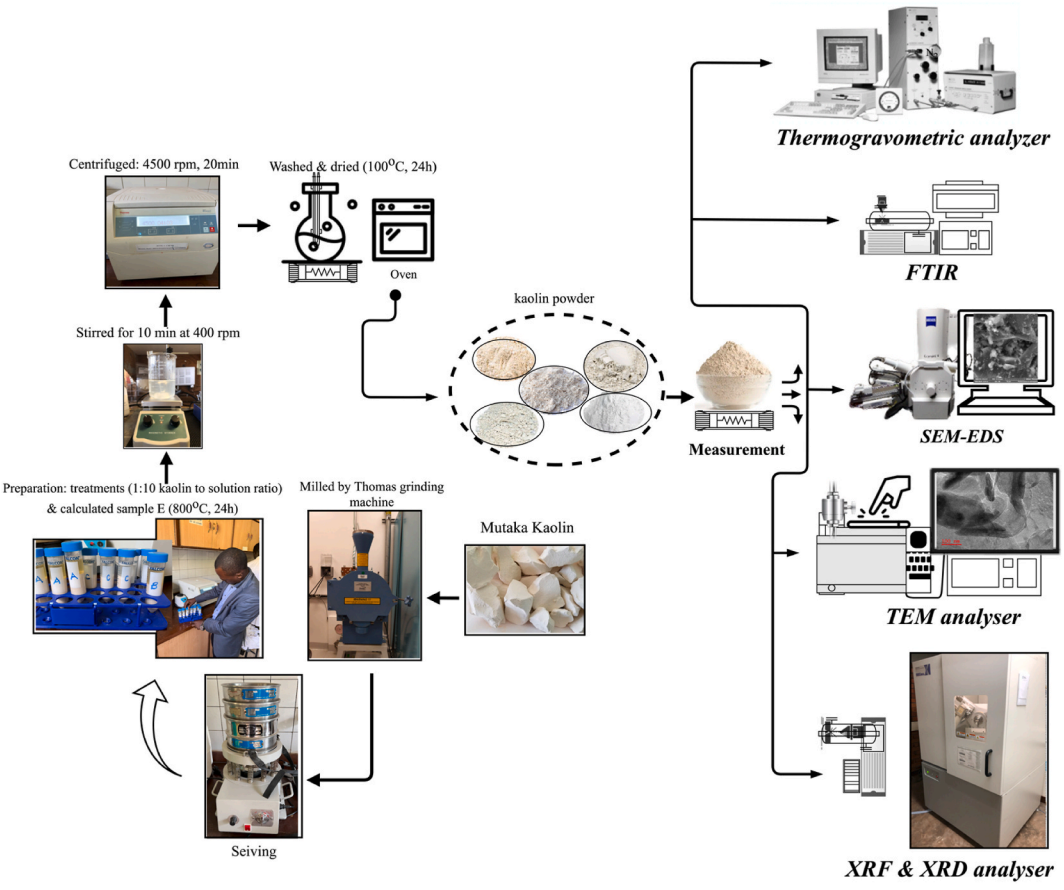

Fig. 1. Experimental process.

evaluation, and their processing are limited in this research. Most research conducted in Uganda regarding kaolin deposits has centered around exploring its use as a reinforcement in composites and pottery, as a source of materials for bricks, and as an insulator [16,20–23]. On the contrary, the potential usefulness of these kaolin deposits for producing paints and coatings has not been considered, which is very important as far as the industrialization of a nation and saving foreign exchange is concerned.

It is crucial to conduct characterization and treatment to improve raw materials' physical and chemical properties. These are particularly important in optimizing the raw materials for specific applications, including creating coatings and paints with desired properties and improved stability. Previous studies have predominantly examined treatment or beneficiation methods for the kaolin [15,24–29], but few have specifically investigated the impact of different treatment methods on kaolin and characterizing the resulting treated kaolin [14,30,31]. These processes can potentially induce changes in physical and chemical properties, including morphology, crystal structure, particle size distribution, and pH, which can subsequently affect the formation of kaolin [32,33]. Consequently, there is a need for a dedicated study focusing on different treatment methods of kaolin and their effects on characterization to address this research gap. Such a study would contribute valuable insights into the impact of treatment processes on kaolin properties and provide a more comprehensive understanding of its behavior and applicability in various applications.

The objective of the present study is to characterize the Mutaka kaolin deposit located in Mitooma district, southwestern region of Uganda. The focus is on different treatments of kaolin mineral samples and characterizing the resulting treated kaolin. The ultimate aim is to treat and characterize by identifying the promising candidates among various kaolin samples to produce low-cost coating pigments. By characterizing the kaolin and enhancing its properties through treatment, the study seeks to establish the potential of this kaolin deposit as a cost-effective pigment for manufacturing kaolin-based coatings and paints.

2. Materials and methods

2.1. Materials and chemicals

The mineral was collected from the Mutaka kaolin deposit in the Mitooma district, southwestern Uganda. The present study utilized a range of laboratory-grade chemicals, including oxalic acid, ammonium molybdate, and iron standard solution. Using laboratory-grade chemicals ensures high purity and consistency, minimizing the potential for impurities or variations that could affect the accuracy and reliability of the results. Fig. 1 depicts the schematic representation of the experimental procedure layout.

2.2. Milling and particle size distribution

This study used lumpy Mutaka kaolin deposits weighing 1 kg each to prepare powders. A Thomas grinding machine was employed to break up the agglomerates and achieve a finer particle size. The lumpy kaolin deposits underwent grinding to facilitate the size reduction process. Subsequently, the kaolin deposit was further processed in a cascading ball mill, using alumina balls as grinding media. This milling step aimed to reduce the particle size of the kaolin further and obtain fine powders suitable for subsequent characterization and beneficiation processes.

Following the milling process, the particle size distribution of the kaolin powders was examined using a TSS-200 vibratory sieve shaker. The sieve shaker was equipped with a four-stack sieve setup arranged according to the ISO 3310 standard. The nominal aperture sizes of the sieves used were 600 μm, 300 μm, 200 μm, and 150 μm, with the sequence from top to bottom. The sieve shaker was operated for 10 min to assess the extent of milling achieved for the Mutaka kaolin samples. After the sieving process, the sets of powders that passed through the sieves with aperture sizes below 150 μm were selected for further analysis.

2.3. Treatment of kaolin

After the milling and particle size distribution analysis, the kaolin particles that passed through the 150 μm size sieve were carefully stored in a dry vacuum environment. The study involved five different treatments of the kaolin samples, namely, (i) oxalic acid treatment, (ii) ammonium molybdate treatment, (iii) beneficiated or de-ionized water treatment, (iv) untreated, and (v) thermal treatment.

2.3.1. Oxalic acid treatment

In this treatment, the kaolin sample was subjected to a concentration of 0.1 M oxalic acid in a solid-to-acid solution ratio of 1:10. The mixture was carried out in a 500 ml Pyrex® flask and stirred at 400 rpm for 20 min using a magnetic stirrer at 23 °C. After mixing the kaolin and oxalic acid solution, the resulting mixture was transferred into Falcon® tubes. The tubes were then centrifuged using a Megafuge™ 8 centrifuge at 4500 rpm for 10 min [31]. The supernatant, which contained the liquid portion of the mixture, was discarded, while the residue product, which consisted of the treated kaolin, remained in the Falcon® tubes. The residue was washed repeatedly with distilled water to remove unspent oxalic acid and other impurities. After the washing step, the kaolin sample was dried at 100 °C for 24 h. The treated sample was designated as sample A.

2.3.2. Ammonium molybdate treatment

Kaolin was treated with a solution containing small quantities of ammonium molybdate, utilizing a ratio of 1:10 (w/v). The resulting mixture was stirred and kept at a constant temperature of 23 °C for 20 min. Following this, the suspensions were subjected to centrifugation at 4500 rpm for 10 min, leading to the separation of the liquid supernatant, which was subsequently discarded. The

sample was then thoroughly washed with distilled water and dried following the procedure outlined in section 2.3.1. The kaolin sample treated in this manner was designated as sample B.

2.3.3. Beneficiated treatment

To ensure homogeneous mixing, 100 g of kaolin was added to deionized water and stirred for 20 min. Subsequently, the dispersion underwent centrifugation at 4500 rpm for 10 min, effectively separating the solid particles. The resulting sediment was subjected to multiple rinses with deionized water to remove residual impurities. Finally, the sample was dried at 100 °C for 24 h to achieve a complete moisture removal [31]. The dried samples were well-mortared for subsequent characterizations. The treated sample was designated as sample C.

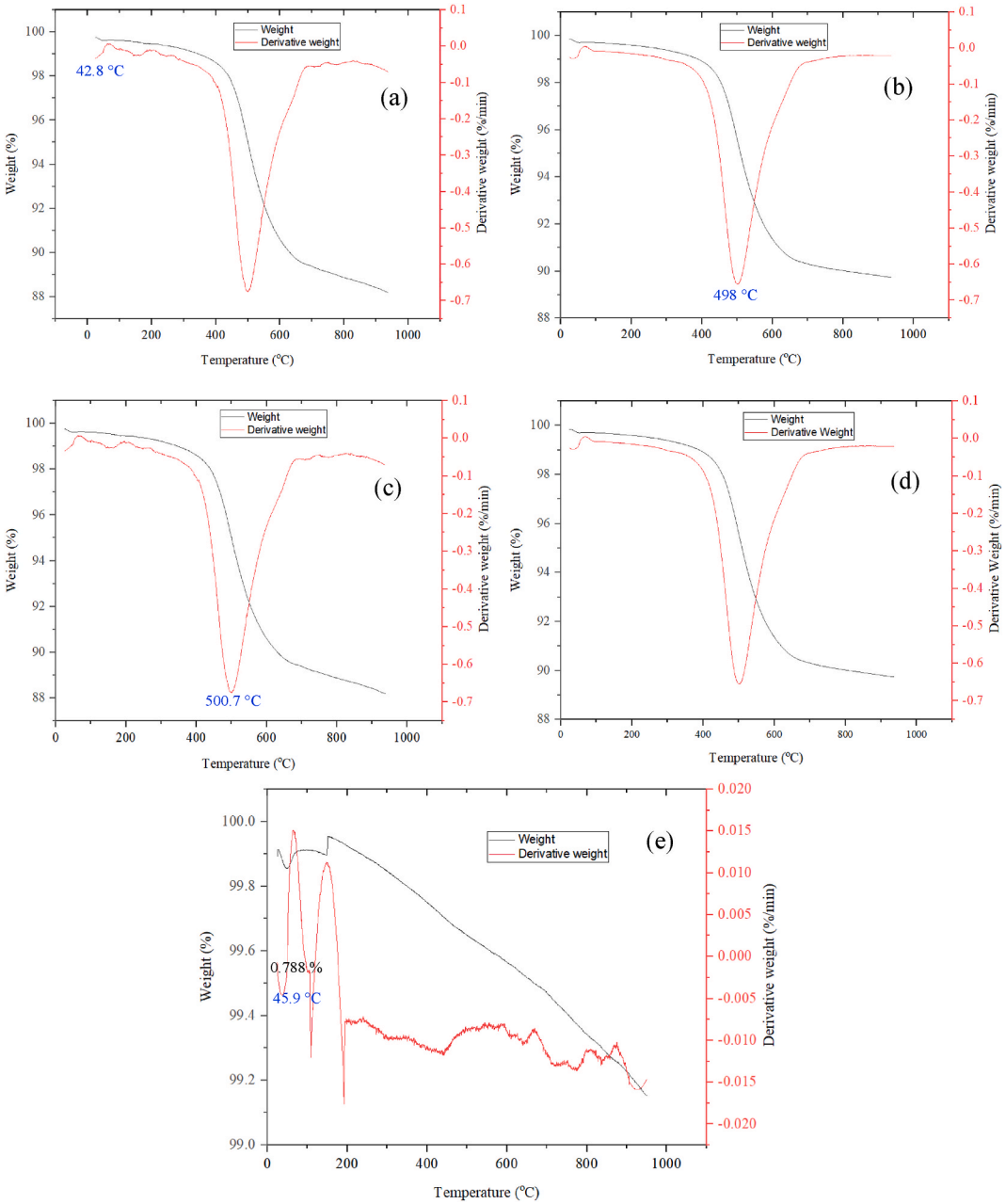

Fig. 2. TGA curves of (a) oxalic acid treated, (b) ammonium molybdate treated, (c) deionized water treated, (d) untreated kaolin, and (e) thermal treated kaolin.

2.3.4. Untreated and thermal treatment

After milling and particle size distribution analysis, 100 g of kaolin particles that passed through a 150 μm sieve were carefully stored as sample D, which served as an untreated sample. Another 100 g of kaolin was subjected to thermal treatment using a Carbolite Gero HTF electric furnace at a temperature of 800 °C for 4 h, without nitrogen (N2) or airflow [33]. The sample remained inside the furnace until it cooled down to approximately 100 °C, and then it was further cooled in a desiccating chamber. The thermally treated sample was labeled as sample E.

2.4. Characterization of kaolin samples

2.4.1. Thermogravimetric (TGA) analysis

The thermal analyses of both treated and untreated samples were determined using a TGA (SDT Q600 V20.9 Build 20), and it shows the relationship between changes in the weight of materials with time as heat is applied. The sample was weighed (~5 mg) and transferred into crucibles by heating it from ambient temperature to 1000 °C at 10 °C per minute under N_2 atmosphere. Furthermore, the degree of conversion of the kaolinite dehydroxylation reaction was determined by analyzing the weight loss of the samples during calcination and the loss on ignition obtained from TGA analysis.

2.4.2. X-ray diffraction (XRD) analysis

Before conducting *p*-XRD analysis, the samples underwent a process of fine pulverization to ensure optimal effectiveness during the investigation. The diffraction patterns were then measured using a Philips X' Pert Pro *p*-XRD instrument. The scan speeds were set at 10°/min, and the data was captured with a resolution of 0.02°. For the analysis, a Cu K α1 radiation source with a wavelength of 1.54 nm was utilized. The instrument was operated at a voltage of 40 kV and a current of 40 mA. Wide-angle measurements were conducted from 10 to 90° (2θ).

2.4.3. Fourier transform infrared (FTIR) analysis

The functional groups present in the samples were determined using an FTIR spectrometer model 4100 from Shimadzu. The FTIR analysis was conducted in the solid state, and small fragments of each silica sphere were powdered and deposited on the attenuated total reflectance (ATR) system for subsequent data acquisition. The wavenumber range explored during the analysis was from 4000 to 500 cm^{-1}.

2.4.4. Transmission electron microscopic (TEM) analysis

TEM analyses were conducted using a Jeol JEM-2100F TEM machine equipped with a LaB6 source. To prepare the TEM samples, a small amount of the synthesized material was placed onto a TEM grid (Cu-grid) with a 200 mesh size, which had been coated with a thin carbon film. The TEM machine operated at an acceleration voltage of 200 kV. The images of the samples were captured using a digital charge-coupled device (CCD) camera connected to the transmission electron microscope.

2.4.5. SEM/EDS analysis

The SEM measurements were conducted utilizing a Tescan Vega 3 LMH instrument. The SEM operated at an accelerating voltage of 20 kV and employed a secondary electron detector (SE). Additionally, the SEM was equipped with energy dispersive spectroscopy (EDS) capabilities. To enhance the conductivity of the materials, they were initially carbon-coated using the Agar Turbo Carbon coater.

3. Results and discussion

3.1. Thermal analysis

Fig. 2(a) and (c) exhibit similar trends in the TGA and differential thermal analysis (DTA) curves, depicting the weight loss and endothermic peaks of kaolin samples treated with oxalic acid and de-ionized water. In the DTA curve, two distinct endothermic peaks were observed. The first endothermic peak, detected at 42.8 °C within the 20–100 °C temperature range, corresponds to removing absorbed water from the surface pores. Reducing the moisture content in kaolin, it becomes more stable and less prone to moisture-related issues, which is crucial for its use in coatings where moisture can lead to defects and reduced performance [34]. The second endothermic peak, observed at 500.7 °C within the temperature range of 495–505 °C, is attributed to the dehydroxylation of minerals within the sample, which results in the formation of amorphous metakaolinite, a property desirable in coating applications [35,36]. These peaks are accompanied by TGA weight loss between 9.208 and 9.766 wt%.

Additionally, metakaolinite is a more reactive form of kaolin, and its presence can enhance the reactivity and performance of kaolin as an additive in coatings. It contributes to improved binding and adhesion properties, which are essential for coating applications [37]. However, the obtained curves suggest that during the gradual heating of the kaolin samples, the following processes and reactions occur successively [38]:

$$Al_2O_3{\cdot}2SiO_2{\cdot}2H_2O\ (\text{kaolinite}) \rightarrow Al_2O_3{\cdot}2SiO_2\ (\text{amorphous metakaolinite}) + 2H_2O$$

This reaction represents the dehydroxylation of kaolinite, which is characterized by endothermic peaks observed in the temperature range of 500–590 °C. As a result of dehydroxylation, water molecules are released, leading to the formation of amorphous

metakaolinite.

Fig. 2(b) and (d) showcases similar trends in the TGA and DTA curves, representing the weight loss and corresponding peaks of sample B (treated with ammonium molybdate) and sample D (untreated sample). In the TGA curve, three distinct endothermic peaks were identified. The first endothermic peak corresponds to the removal of adsorbed water, the second peak signifies the decomposition of impurities, and the third peak indicates the dehydroxylation reaction of the kaolin. The total weight loss observed was between 11.15 and 11.34 %, occurring until a temperature of 498 °C. The rapid evaporation of water might lead to an accumulation of small binder particles in the coating surface layer, thereby creating porosity and surface energy differences due to local variations in thickness and density [39]. An exothermic peak was detected within the 635–970 °C temperature range. This peak likely indicates a phase transformation occurring from metakaolin to spinel formation. Notably, no discernible mass loss was observed throughout this phase transformation process. These thermal analysis results align with findings reported in the literature by Refs. [40,41]. As the temperature increases further, the kaolin transforms into a crystalline phase, as described by the equation:

$$Al_2O_3\ 2SiO_2 \longrightarrow 2Al_2O_3\ 3SiO_2 + SiO_2\ H_2O \text{ amorphous} + \gamma\ Al_2O_3$$

This transformation is accompanied by an exothermic peak between 800 and 1000 °C.

A low weight loss of 0.788 % was observed for sample E when heated at 45.9 °C (see Fig. 2(e)). This indicates that the thermally treated kaolin experienced minimal mass loss at this temperature. The crystallinity of kaolinite is known to be predominantly lost around 600 °C. The kaolinite structure changes at this temperature, and the original hexagonal layer structure becomes disorganized. This structural transformation contributes to the low mass loss observed in the thermally treated kaolin sample.

3.2. XRF analysis

As presented in Table 1, the XRF analysis results indicate variations in the composition of SiO_2 and Al_2O_3, ranging from 41.70 % to 49.98 % and 35.17 %–39.20 %, respectively. The loss on ignition, which represents the amount of organic and volatile compounds, varied between 9.60 % and 17.36 %. These values were closest to the theoretical kaolin composition, suggesting that the kaolinite was enriched after clay description and classification. The high SiO_2 content observed in all raw kaolin samples indicates that SiO_2 is the primary oxide present, followed by Al_2O_3 [42]. In this study, a small amount of TiO_2 (0.004 %) was detected in the kaolinite-rich samples, which is even lower than the amounts reported in the literature. High levels of TiO_2 can affect the whiteness and brightness of kaolin when used in paint and coating applications.

3.3. XRD analysis

The untreated kaolin samples and those treated with oxalic acid, ammonium molybdate, and de-ionized water exhibit well-defined diffractions at specific 2θ values (see Fig. 3). These peaks, observed at 2θ values of 12.20–12.45°, 20.02–20.19°, 24.82–21.01°, 37.89°, 55.04°, and 63.1°, are typically associated with kaolinite [25,30]. The diffraction patterns of all kaolin samples also reveal peaks at 2θ values of 20.82–21.65°, 27.38°, and 30.03°, which are characteristic of K-feldspar, except sample E. However, the highest intensity peaks of quartz are observed at 26.74–27.02° of 2θ values. This stability is crucial in coatings to ensure the additive's properties remain consistent. These findings are consistent with previous studies [47–49] that reported these peaks as associated with quartz. Compared to sample E, the x-ray diffraction patterns obtained in samples A, B, C, and D indicate that samples are rich in kaolinite, K-feldspar, and quartz, which provides a range of properties that can benefit coatings.

The acid treatment (sample A) applied to the kaolin samples did not significantly impact the primary reflections of the kaolin minerals, as evidenced by the XRD diffraction patterns. Compared to the other treated samples, the thermal treatment (sample E) resulted in a notable change, as depicted in Fig. 3. The XRD diffraction peaks associated with kaolin minerals disappeared, while the K-feldspar peak remained visible in the calcined kaolinite. This indicates that the thermal modifications at 800 °C caused the absence of kaolin d_{001} reflections, regardless of whether they originated from major halloysite, kaolinite, or included their iron oxide impurities. Different treatments had varying impacts on these minerals. Notably, thermal treatment resulted in the transformation of kaolinite into metakaolin, which is essential for enhancing certain coating properties.

Table 1
XRF composition of untreated kaolin and those reported in the literature.

Oxides	Chemical composition (% w/w)										
	SiO_2	Al_2O_3	Fe_2O_3	CaO	MgO	K_2O	Na_2O	TiO_2	P_2O_5	LOI	Reference
Raw Indian Kaolin	45.22	38.43	0.52	0.04	0.033	0.84	0.18	0.269	0.03	12.00	[43]
Raw Algerian Kaolin	41.70	35.80	0.801	1.16	0.183	0.301	N. D	0.070	N. D	17.364	[44]
Raw Ghanaian Assin-Fosu Kaolin	49.79	35.17	0.76	0.200	1.14	0.60	2.14	0.14	0.03	9.6	[45]
Raw Ugandan Buvumbo Kaolin	49.98	35.97	0.34	<0.01	0.33	0.99	0.025	0.02	0.06	12.61	[21]
Raw Ugandan Migade Kaolin	49.90	35.62	0.54	<0.01	0.34	0.78	0.044	0.05	0.11	12.85	[21]
Raw Ugandan Mutaka Kaolin	48.80	36.00	0.238	0.09	0.038	1.14	0.004	0.004	0.009	12.60	This study
Beneficiated Ugandan Mutaka Kaolin	45.20	39.20	0.417	0.135	0.059	0.760	<0.040	0.012	0.002	13.70	[46]

LOI-Loss on ignition in weight %, N. D-no data.

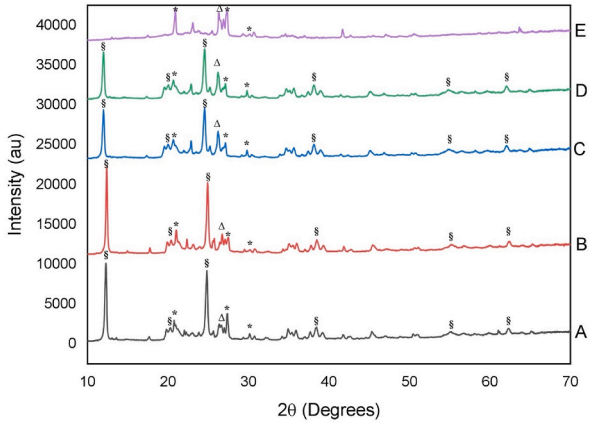

Fig. 3. XRD spectrum of untreated and treated samples. § = kaolin; * = K-feldspar; Δ = quartz.

3.4. FTIR analysis

Fig. 4 depicts the FTIR spectra of untreated kaolin and the samples treated with oxalic acid, ammonium molybdate, heat, and deionized water. In Fig. 4(a)–4(d), the FTIR results show that the OH stretching vibrations are observed in the wavenumber range of 3707 to 3576 cm^{-1}. These hydroxyl groups can potentially interact with other components in coatings, enhancing adhesion and performance. Within the range of 1200-500 cm^{-1} (refer to Fig. 4(a)–(d)), the γSi-O stretching vibrations of kaolinite exhibit distinct peaks at 1103, 1094, 980, and 847 cm^{-1}. These frequencies correspond to the specific molecular vibrations of kaolinite. Additionally, the FTIR spectrum of the samples reveals a prominent band at 779 cm^{-1}, which can be attributed to quartz, based on previous studies [31,50]. Furthermore, an intensity band observed at 947 cm^{-1} is associated with the Al–Al–OH groups present in the sample. This band provides information about the presence of these particular chemical groups. Moreover, the bands detected at 606 and 589 cm^{-1} correspond to the γSi-O stretching vibrations, as reported in a study by Ref. [51]. Additionally, the band observed at 503 cm^{-1} corresponds to the γSi-*O*-Al stretching vibrations. These spectral features suggest the presence of illite and K-feldspars in the sample, consistent with the results obtained from XRD analysis.

Fig. 4(e) illustrates the thermal treatment of the kaolinite sample, resulting in the formation of metakaolin at 800 °C. The figure shows that the sharp OH bands, typically in the OH-stretching band range of 2500–3800 cm^{-1}, vanish entirely. This disappearance is evident in Fig. 4(e). Additionally, the bands at 1110-980 cm^{-1}, corresponding to Si–O stretching vibrations, and those at 847 and 779 cm^{-1} also cease to exist. These findings are consistent with the X-ray diffraction (XRD) results, indicating the destruction or alteration of the kaolinite structure as a consequence of the thermal treatment (heating to 800 °C). The changes in the infrared (IR) spectral features align with the XRD data, affirming the transformation of kaolinite into metakaolin due to the applied thermal conditions.

3.5. SEM-EDS analysis

The SEM images in Fig. 5 display different treated and untreated kaolin samples and reveal certain observations and comparisons. Compared to the oxalic acid leaching process (Fig. 5(a)), sample E and sample B formed a more porous structure. This finding is consistent with the literature reported by Refs. [30,52]. Increased porosity can enhance the material's ability to absorb and hold onto other coating components. This can lead to better dispersion of pigments, binders, and other additives, improving the overall performance and coverage of the coating [53]. In contrast, untreated kaolin may have a less porous structure, making it less effective at absorbing and holding onto these components. A recent investigation showed that the porosity increased with increasing kaolin in the coating layer [39]. Additionally, the thermal treatment applied to the Mutaka kaolin (sample E) resulted in significant modifications, as evident in the EDS compositions presented in Table 2. This treatment caused dehydroxylation, producing amorphous metakaolin from the Mutaka mineral, as described by Ref. [33]. Regarding the beneficiation and untreated kaolin results, the SEM images in Fig. 5 (c) and (e) indicate that larger kaolin particles were fragmented, resulting in fewer aggregations and the formation of a platelet structure. This structural change led to an increase in surface area. Both micrographs, Fig. 5(c) and (e), demonstrate a disorderly arrangement of particles, suggesting a generally amorphous nature. Furthermore, these particles appear dispersed alongside crystalline silica particles.

Fig. 6, which displays the EDS layered images, provides insights into the interaction of various elements and electrons within the kaolin matrix. The EDS analysis of all samples indicates a significant and intimate mixture of silicon (Si) and aluminum (Al) throughout the kaolin samples, suggesting preserving the original kaolin structure despite the different treatments.

Table 2 presents the results of the EDS analysis, showing a notable reduction in silicon content in the raw kaolin sample after undergoing treatments with deionized water, thermal treatment, oxalic acid, and ammonium molybdate. The silicon weight percentages are reported as follows: 26.5 wt% for raw kaolin, 23.6 wt% for beneficiated kaolin, 22.2 wt% for thermally treated kaolin, 17.6 wt% for kaolin treated with oxalic acid, and 21.9 wt% for kaolin treated with ammonium molybdate. This reduction in silicon

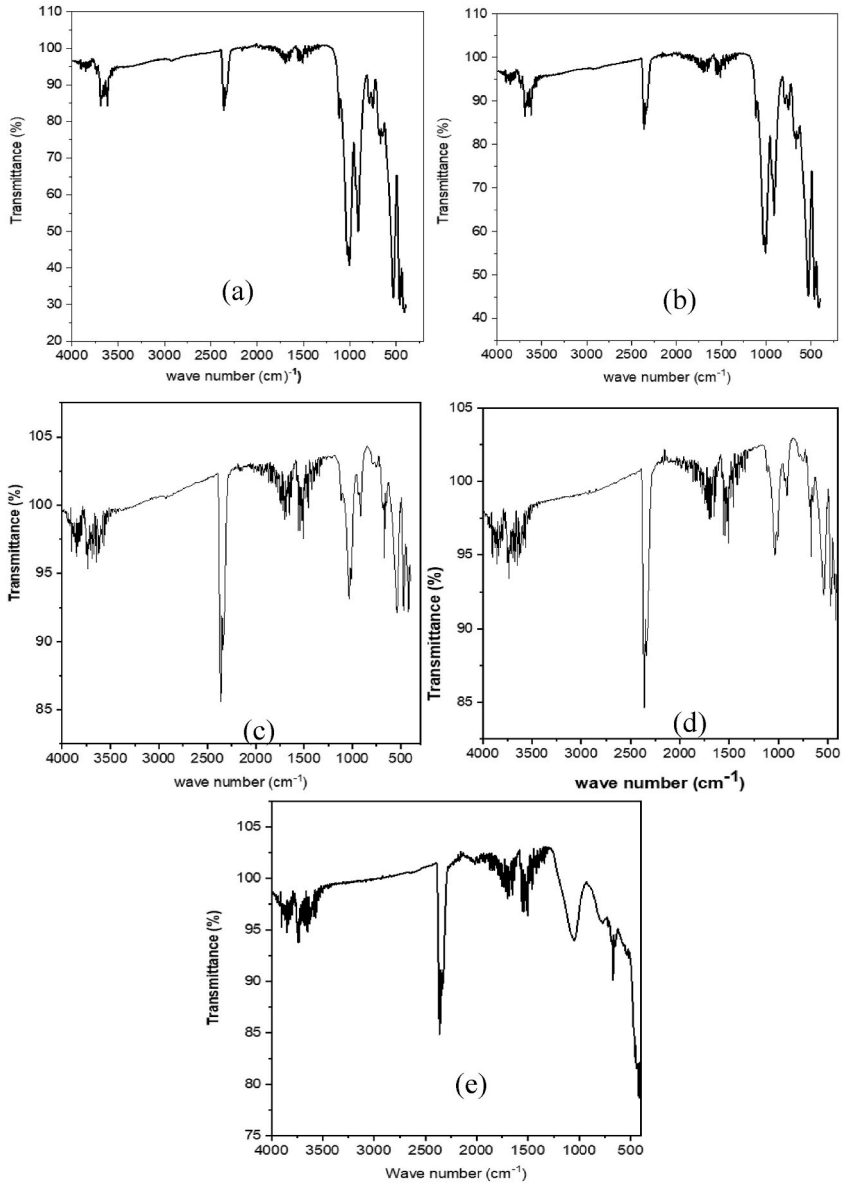

Fig. 4. FTIR spectrum of (a) oxalic acid treated, (b) ammonium molybdate treated, (c) deionized water treated, (d) untreated kaolin, and (e) thermal treated kaolin.

content indicates a decrease in the amount of sand, which is a major impurity in kaolin. The lower silicon content is desirable, as it reduces impurities and increases the whiteness of the additive for coating.

In the case of potassium (K), the high reactivity of this element during heating leads to a decrease in its concentration compared to raw kaolin. Specifically, the concentration of K decreases from 9.1 wt% in raw kaolin to 8.0 wt% after heating. Also, when treated with oxalic acid, which is a weak acid, the alkaline elements, including K, undergo reactions that reduce their concentration. The increased concentration of oxygen observed in the elemental analysis is representative of the strong bonds formed from silica and alumina. These elements contribute to the formation of stable bonds within the kaolin structure. This reduction can be beneficial for coatings, as the high reactivity of potassium during heating may lead to undesirable reactions that affect coating properties. Additionally, when alkaline elements react with the acidic-leaning elements, such as Al, the concentration of the acidic elements decreases. This is the case for Al, which experiences a reduction in concentration when it reacts with alkali. The effervescent reaction of ammonium molybdate with kaolin causes a subsequent decrease in the concentration of highly reactive K. As a result, the concentration of K is further reduced in this treatment.

Furthermore, the decrease in impurities, particularly iron oxide, contributes to the whiteness observed in the treated kaolin samples compared to the raw kaolin. This reduction in iron oxide impurity is crucial for kaolin's application as a filler material in paint. The

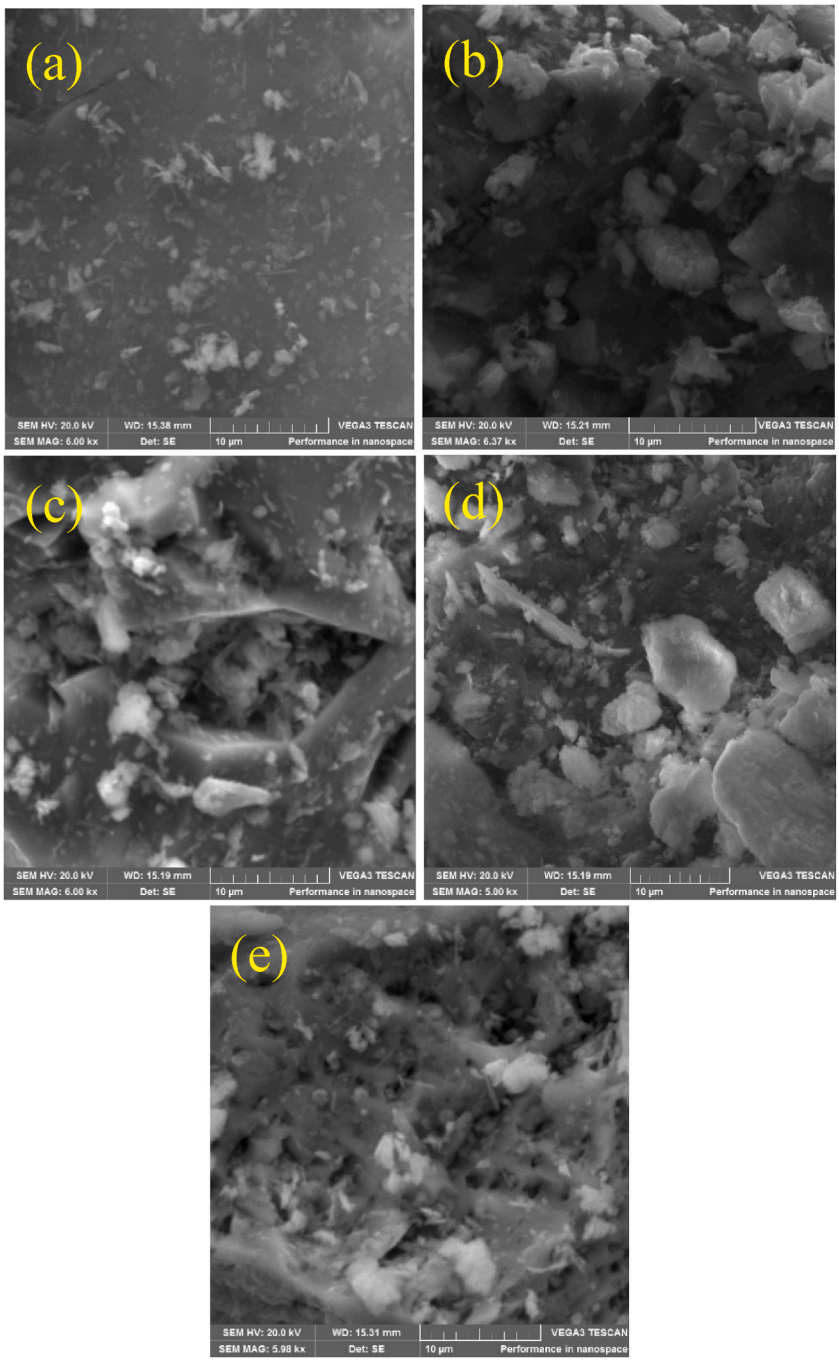

Fig. 5. SEM images at a spatial resolution of 10 µm for (a) oxalic acid treated, (b) ammonium molybdate treated, (c) deionized water treated, (d) untreated kaolin, and (e) thermal treated kaolin.

whiteness of kaolin is an important property in paint applications, and thus, the treatment of raw kaolin is necessary to achieve the desired whiteness when used as a filler material [34]. The high oxygen weight percentage in the EDS analysis represents hydroxide groups contributing to the kaolin structure bonding. The treatments of raw kaolin generally reduce the number of oxygen bonds, indicating a decrease in hydroxide groups. However, the oxalic acid treatment stands out as it provides additional hydroxyl groups to the kaolin matrix, increasing oxygen bonds.

Table 2
Elemental composition of kaolin samples by EDS.

Elements	Sample A		Sample B		Sample C		Sample D		Sample E	
	wt%	σ	wt%	Σ	wt%	σ	wt%	σ	wt%	σ
O	52.8	0.5	47.2	0.7	39.5	1.0	51.5	0.4	44.4	1.4
Si	17.6	0.2	21.9	0.4	23.6	0.6	26.5	0.3	22.2	0.7
Al	16.3	0.2	13.4	1.2	15.4	1.8	12.9	0.2	14.3	2.3
C	8.9	0.8	9.5	0.2	12.7	0.4	–	–	11.1	0.4
K	4.4	0.1	8.0	0.2	8.7	0.3	9.1	0.2	8.0	0.4

Note: σ-standard deviation.

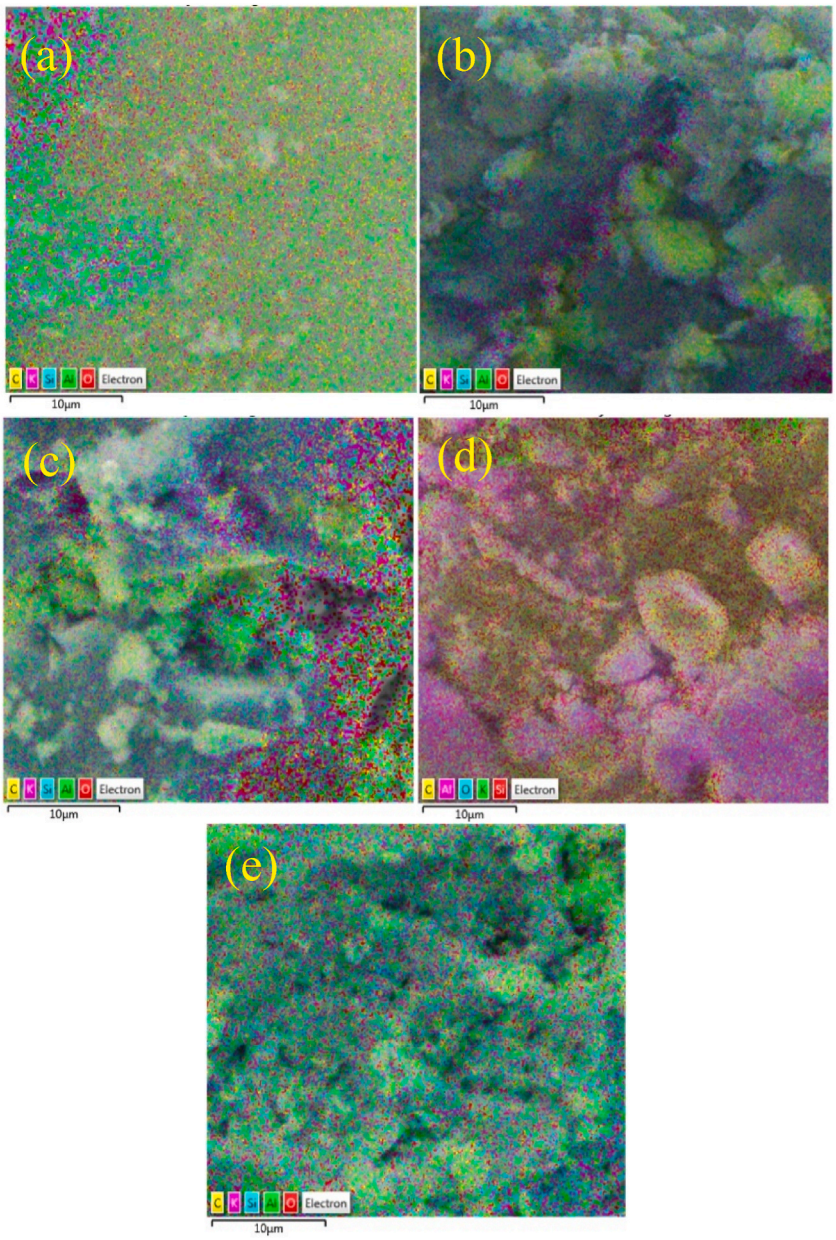

Fig. 6. EDS mappings at a spatial resolution of 10 μm for (a) oxalic acid treated, (b) ammonium molybdate treated, (c) deionized water treated, (d) untreated kaolin, and (e) thermal treated kaolin.

3.6. TEM analysis

Fig. 7(a)-(e) displays TEM micrographs and crystalline structures of kaolin samples subjected to different treatments. In all the images, the hexagonal nature of kaolinite platelets is visibly apparent. This characteristic is attributed to the crystal structure of kaolinite, which comprises stacked layers of aluminum octahedra and silicon tetrahedra. Notably, certain layers within the structure adopt a hexagonal arrangement, giving rise to platelets with a hexagonal shape (refer to Fig. 7(a)-(b) and 7(d)–(e)). In Fig. 7(a), the micrograph provides a distinct view of the kaolin nanoparticles, exhibiting an amorphous characteristic with an average size distribution of 23 nm. The micrograph also reveals individual crystals in the form of flakes, showcasing a pseudohexagonal morphology.

Moving to Fig. 7(b)–a noticeable distinction can be observed, with a clearer and more organized arrangement of particles resulting from the mass concentration of kaolin. This is evident from the dark shades in the TEM image, particularly after treatment with ammonium molybdate, compared to the untreated kaolin sample. We also noticed a significant increase in kaolinite flakes peeled off as layers in the ammonium molybdate-treated samples. This observation suggests that the treatment with ammonium molybdate had a pronounced effect on the delamination and exfoliation of the kaolinite layers, separating individual platelets or flakes. These changes can contribute to the dispersibility and homogeneity of kaolin in coatings. Furthermore, Fig. 7(e) presents sample E, which exhibits good crystallinity, solid growth, and a cubic morphology, accompanied by a uniform size distribution. This finding aligns with the literature discovered by Ref. [54]. These crystalline shapes and the random nature of the structure lead to high absorptivity and porosity of the mineral, which are characteristics that lead to easy wettability in liquid systems [34].

4. Conclusion

This study aims to assess, treat, and characterize the promising candidates among various kaolin samples for producing low-cost coating pigments. From the results, the following conclusions were obtained.

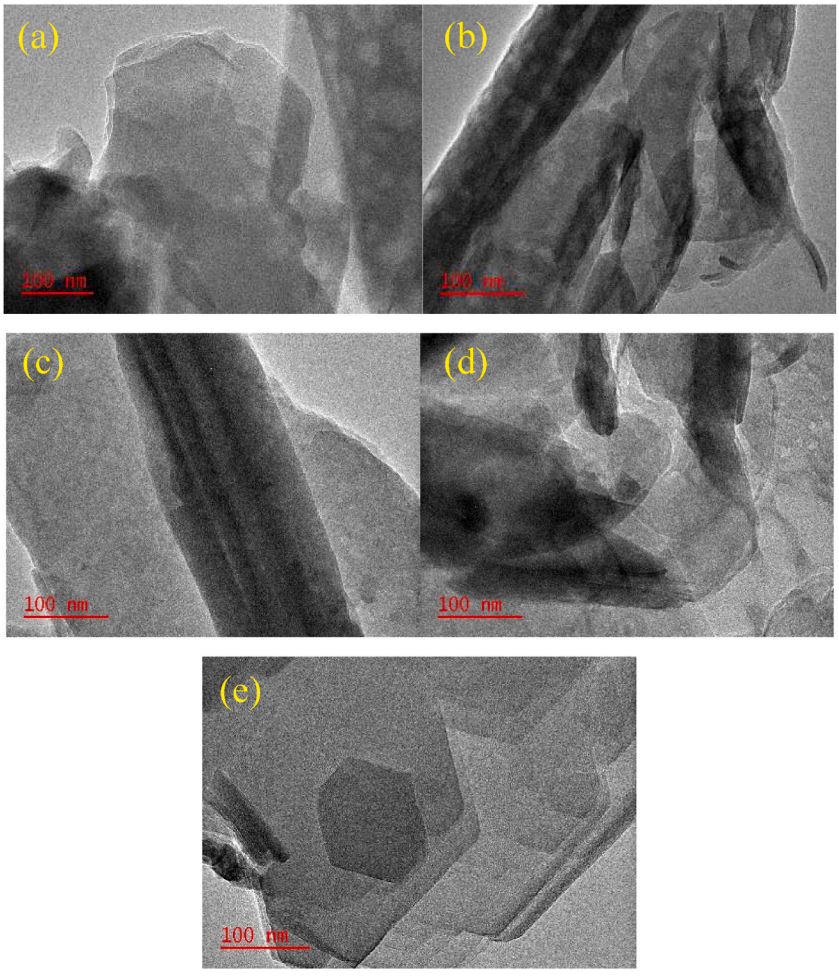

Fig. 7. TEM images of (a) oxalic acid treated, (b) ammonium molybdate treated, (c) deionized water treated, (d) untreated kaolin, and (e) thermal-treated kaolin.

1. Sample E exhibits minimal mass loss at 45.9 °C, indicating the thermal treatment had limited impact. The crystallinity of kaolinite is lost around 600 °C, resulting in structural changes and low mass loss in the treated sample.
2. The loss on ignition, representing organic and volatile compounds, ranges from 9.60 to 17.36 %. These values closely resemble the composition of theoretical kaolin, suggesting the enrichment of kaolinite after clay description and classification. The high SiO_2 content indicates it is the primary oxide, followed by Al_2O_3. Trace amounts of TiO_2 were detected in the kaolinite-rich samples, lower than reported in the literature.
3. Acid treatment does not significantly affect the primary reflections of the kaolin minerals in the XRD patterns. However, thermal treatment results in the disappearance of kaolin mineral peaks while the K-feldspar peak remains visible. This indicates that the thermal modifications cause the absence of kaolin reflections, leading to the transformation of kaolinite into metakaolin, which can enhance coating properties.
4. Sample A to D shows a band indicating quartz's presence at 779 cm^{-1}, while the Al–Al–OH groups are associated with an intensity band at 947 cm^{-1}. In the 1200-500 cm^{-1} and 606-589 cm^{-1} range, the bands correspond to γSi-O stretching, and the band at 503 cm^{-1} corresponds to γSi-*O*-Al stretching. These bands suggest the presence of illite and K-feldspars, as confirmed by XRD patterns. In sample E, the OH bands and Si–O stretching bands disappear completely, indicating the destruction of the kaolinite structure due to the thermal effect.
5. Sample B and E show a more porous structure than sample A. Sample D leads to significant modifications in Mutaka kaolin, producing amorphous metakaolin. Sample C and E exhibit fragmentation of larger particles, forming a platelet structure and increasing surface area. The treatments also reduce iron oxide impurity, resulting in whiter kaolin, which can positively impact coating properties, including adhesion and performance.
6. All the TEM images confirm the hexagonal nature of kaolinite platelets and reveal the amorphous nature of the kaolin nanoparticles with sample A. Treatment with ammonium molybdate enhances particle arrangement and causes increased delamination of kaolinite layers, improving dispersibility and homogeneity in coatings. Sample E shows desirable characteristics with good crystallinity, solid growth, cubic morphology, and uniform size distribution.

While other treatments had their benefits and modified specific properties of kaolin, the thermal treatment demonstrated a unique set of advantages, including high thermal stability and structural transformation. These qualities make it a promising candidate as an additive in coatings, as it can potentially enhance the coating's performance and durability, especially under elevated temperature conditions.

Additional information

No additional information is available for this paper.

CRediT authorship contribution statement

Andrew Kasumba Buyondo: Conceptualization, Data curation, Formal analysis, Investigation, Methodology, Visualization, Writing - original draft, Writing - review & editing, Funding acquisition. **Hillary Kasedde:** Data curation, Supervision, Validation, Writing - original draft. **John Baptist Kirabira:** Formal analysis, Funding acquisition, Supervision, Validation, Visualization. **Ocident Bongomin:** Validation, Visualization, Writing - review & editing.

Declaration of competing interest

The authors declare that they have no known competing financial interests or personal relationships that could have appeared to influence the work reported in this paper.

References

[1] S. Raj, Global Construction Paints and Coatings Market Is Estimated to Account for US$ 119,451.1 Mn by End of 2027, Says Coherent Market Insights (CMI) | Business Wire, 2020. https://www.businesswire.com/news/home/20200902005395/en/Global-Construction-Paints-and-Coatings-Market-Is-Estimated-to-Account-For US-119451.1-Mn-by-End-of-2027-Says-Coherent-Market-Insights-CMI. (Accessed 22 December 2021).
[2] K.A. Buyondo, H. Kasedde, J.B. Kirabira, A comprehensive review on kaolin as pigment for paint and coating: recent trends of chemical-based paints, their environmental impacts and regulation, Case Stud. Chem. Environ. Eng. 6 (2022), https://doi.org/10.1016/j.cscee.2022.100244.
[3] A.A. Yusuf, J.D. Ampah, I. Veza, A.E. Atabani, A.T. Hoang, A. Nippae, M.T. Powoe, S. Afrane, D.A. Yusuf, I. Yahuza, Investigating the influence of plastic waste oils and acetone blends on diesel engine combustion, pollutants, morphological and size particles: dehalogenation and catalytic pyrolysis of plastic waste, Energy Convers. Manag. 291 (2023) 117312, https://doi.org/10.1016/j.enconman.2023.117312.
[4] T. Häkkinen, P. Ahola, L. Vanhatalo, A. Merra, Environmental Impact of Painted Exterior Wooden Cladding, VTT Julk., 1999, pp. 1–84.
[5] International Agency for Research on Cancer, IARC Monographs on the Identification of Carcinogenic Hazards to Humans - Preamble, World Heal. Organ., 2019, pp. 1–44. https://monographs.iarc.who.int/list-of-classifications. (Accessed 24 October 2021).
[6] V.J. Cogliano, R. Baan, K. Straif, Y. Grosse, B. Lauby-Secretan, F. El Ghissassi, V. Bouvard, L. Benbrahim-Tallaa, N. Guha, C. Freeman, L. Galichet, C.P. Wild, Preventable exposures associated with human cancers, J. Natl. Cancer Inst. 103 (2010) 1827–1839, https://doi.org/10.1093/jnci/djr483.
[7] T. Brown, A. Darnton, L. Fortunato, L. Rushton, Occupational cancer in britain, Br. J. Cancer 107 (2012) S56–S70, https://doi.org/10.1038/bjc.2012.119.
[8] T. Greiner, V. Veleva, A. Phipps, Paint Product Stewardship- A Background Report for the National Dialogue on Paint Product Stewardship, 2004. https://cdn.ymaws.com/www.productstewardship.us/resource/resmgr/imported/Background_Report_for_the_National_Dialogue_on_Paint.pdf.
[9] Z. Kazi, B.S. Hungund, J.S. Yaradoddi, N.R. Banapurmath, A.A. Yusuf, K.L. Kishore, M.E.M. Soudagar, T.M.Y. Khan, A. Elfasakhany, K.A. Buyondo, Production, characterization, and antimicrobial activity of pigment from streptomyces species, J. Nanomater. 2022 (2022) 1–8, https://doi.org/10.1155/2022/3962301.

[10] A.A. Yusuf, F.L. Inambao, Characterization of Ugandan biomass wastes as the potential candidates towards bioenergy production, Renew. Sustain. Energy Rev. 117 (2020) 109477, https://doi.org/10.1016/j.rser.2019.109477.
[11] A.A. Yusuf, F.L. Inambao, A.S. Hassan, S.S. Nura, V. Karthickeyan, Comparative study on pyrolysis and combustion behavior of untreated Matooke biomass wastes in East Africa via TGA, SEM, and EDXS, Int. J. Energy Environ. Eng. 11 (2020) 265–273, https://doi.org/10.1007/s40095-019-00331-2.
[12] F.A. Morsy, S. El-Sherbiny, M.S. Hassan, H.F. Mohammed, Modification and evaluation of Egyptian kaolinite as pigment for paper coating, Powder Technol. 264 (2014) 430–438, https://doi.org/10.1016/j.powtec.2014.05.040.
[13] A. Elgamouz, N. Tijani, From a naturally occurring-clay mineral to the production of porous ceramic membranes, Microporous Mesoporous Mater. 271 (2018) 52–58, https://doi.org/10.1016/j.micromeso.2018.05.030.
[14] L.M. Romero-Guerrero, R. Moreno-Tovar, A. Arenas-Flores, Y. Marmolejo Santillán, F. Pérez-Moreno, Chemical, mineralogical, and refractory characterization of kaolin in the regions of huayacocotla-alumbres, Mexico, Adv. Mater. Sci. Eng. 2018 (2018) 1–11, https://doi.org/10.1155/2018/8156812.
[15] A. Mamudu, M. Emetere, D. Okocha, S. Taiwo, F. Ishola, F. Elehinafe, E. Okoro, Parametric investigation of indigenous Nigeria mineral clay (Kaolin and Bentonite) as a filler in the Fluid Catalytic Cracking Unit (FCCU) of a petroleum refinery, Alexandria Eng. J. 59 (2020) 5207–5217, https://doi.org/10.1016/j.aej.2020.09.050.
[16] K.A. Buyondo, P.W. Olupot, J.B. Kirabira, A.A. Yusuf, Optimization of production parameters for rice husk ash-based geopolymer cement using response surface methodology, Case Stud. Constr. Mater. 13 (2020) e00461, https://doi.org/10.1016/j.cscm.2020.e00461.
[17] M.E. Awad, A. López-Galindo, M. Setti, M.M. El-Rahmany, C.V. Iborra, Kaolinite in pharmaceutics and biomedicine, Int. J. Pharm. 533 (2017) 34–48, https://doi.org/10.1016/j.ijpharm.2017.09.056.
[18] A.J. Bloodworth, D.E. Highley, C.J. Mitchell, Industrial Minerals Laboratory Manual:Kaolin BGS TechnicalReport WG/93/1 (1993) 2014.
[19] American Elements, Kaolin, The Advanced Materials Manufacturer, 2021. https://www.americanelements.com/kaolin-92704-41-1. (Accessed 8 October 2021).
[20] J.B. Kirabira, G. Wijk, S. Jonsson, J.K. Byaruhanga, Fireclay refractories from Ugandan kaolinitic minerals, Steel Res. Int. 77 (2006) 531–536, https://doi.org/10.1002/srin.200606426.
[21] G.W.A. Nyakairu, C. Koeberl, H. Kurzweil, The Buwambo kaolin deposit in Central Uganda: mineralogical and chemical composition, Geochem. J. 35 (2001) 245–256, https://doi.org/10.2343/geochemj.35.245.
[22] P.W. Olupot, S. Jonsson, J.K. Byaruhanga, Study of glazes and their effects on properties of triaxial electrical porcelains from Ugandan minerals, J. Mater. Eng. Perform. 19 (2010) 1133–1142, https://doi.org/10.1007/s11665-010-9597-1.
[23] J.B. Kirabira, S. Jonsson, J.K. Byaruhanga, Beneficiation and evaluation of Mutaka kaolin, Second Int. Conf. Advaces Eng. Technol. (2011) 169–175. https://www.mak.ac.ug/documents/Makfiles/aet2011/Kirabira.pdf.
[24] A. Martínez-Luévanos, M.G. Rodríguez-Delgado, A. Uribe-Salas, F.R. Carrillo-Pedroza, J.G. Osuna-Alarcón, Leaching kinetics of iron from low grade kaolin by oxalic acid solutions, Appl. Clay Sci. 51 (2011) 473–477, https://doi.org/10.1016/j.clay.2011.01.011.
[25] H. Senoussi, H. Osmani, C. Courtois, M. el H. Bourahli, Mineralogical and chemical characterization of DD3 kaolin from the east of Algeria, Boletín La Soc. Española Cerámica y Vidr. 55 (2016) 121–126, https://doi.org/10.1016/j.bsecv.2015.12.001.
[26] M.R. Hosseini, A. Ahmadi, Biological beneficiation of kaolin: a review on iron removal, Appl. Clay Sci. 107 (2015) 238–245, https://doi.org/10.1016/j.clay.2015.01.012.
[27] P.N. Olvera-Venegas, L.E. Hernández Cruz, G.T. Lapidus, Leaching of iron oxides from kaolin: synergistic effect of citrate-thiosulfate and kinetic analysis, Hydrometallurgy 171 (2017) 16–26, https://doi.org/10.1016/j.hydromet.2017.03.015.
[28] P. Zhu, W. Zeng, X. Xu, L. Cheng, X. Jiang, Z. Shi, Influence of acid leaching and calcination on iron removal of coal kaolin, Int. J. Miner. Metall. Mater. 21 (2014) 317–325, https://doi.org/10.1007/s12613-014-0911-z.
[29] M. Gougazeh, Removal of iron and titanium contaminants from Jordanian Kaolins by using chemical leaching, J. Taibah Univ. Sci. 12 (2018) 247–254, https://doi.org/10.1080/16583655.2018.1465714.
[30] T.A. Aragaw, F.T. Angerasa, Synthesis and characterization of Ethiopian kaolin for the removal of basic yellow (BY 28) dye from aqueous solution as a potential adsorbent, Heliyon 6 (2020) e04975, https://doi.org/10.1016/j.heliyon.2020.e04975.
[31] T.M. Zewdie, I. Prihatiningtyas, A. Dutta, N.G. Habtu, B. Van der Bruggen, Characterization and beneficiation of Ethiopian kaolin for use in fabrication of ceramic membrane, Mater. Res. Express 8 (2021) 115201, https://doi.org/10.1088/2053-1591/ac2f75.
[32] M. Arias, Effects of iron and aluminium oxides on the colloidal and surface properties of kaolin, Clays Clay Miner 43 (1995) 406–416, https://doi.org/10.1346/CCMN.1995.0430403.
[33] B. Biswas, M.R. Islam, A.K. Deb, A. Greenaway, L.N. Warr, R. Naidu, Understanding iron impurities in Australian kaolin and their effect on acid and heat activation processes of clay, ACS Omega 8 (2023) 5533–5544, https://doi.org/10.1021/acsomega.2c06795.
[34] D. Brezinski, J.V. Koleske, 2011 additives handbook, PCI-Paint Coatings Ind 27 (2011).
[35] P.S. Kumar, P.K. Nair, X-ray diffraction studies on the relative proportion and decomposition of amorphous phase in electroless NiB deposits, Nanostructured Mater 4 (1994) 183–198, https://doi.org/10.1016/0965-9773(94)90077-9.
[36] Y. Shajari, A. Alizadeh, Z.S. Seyedraoufi, S.H. Razavi, H. Shamakhi, The effect of heat treatment on wear characteristics of nanostructure Ni-B coating on marine bronze, Mater. Res. Express 6 (2019), https://doi.org/10.1088/2053-1591/ab395d.
[37] H. Parmar, Exploring the Properties and Applications of Kaolin, ShreeRam Kaolin, 2023. https://shreeramkaolin.com/exploring-the-properties-and-applications-of-kaolin/. (Accessed 7 October 2023).
[38] R. Deju, A. Cucos, M. Mincu, C. Tuca, Thermal characterization of kaolinitic clay, Rom. J. Phys. 66 (2021) 1–8.
[39] E. Bohlin, Surface and Porous Structure of Pigment Coatings: Interactions with Flexographic Ink and Effects on Print Quality, 2013.
[40] A. Tironi, M.A. Trezza, E.F. Irassar, A.N. Scian, Thermal treatment of kaolin: effect on the pozzolanic activity, Procedia Mater. Sci. 1 (2012) 343–350, https://doi.org/10.1016/j.mspro.2012.06.046.
[41] A.E. Kassa, N.T. Shibeshi, B.Z. Tizazu, S.V. Prabhu, Characteristic investigations on Ethiopian kaolinite: effect of calcination temperature on pozzolanic activity and specific surface area, Adv. Mater. Sci. Eng. 2022 (2022) 1–8, https://doi.org/10.1155/2022/2481066.
[42] N.H. Jamil, M.M.A.B. Abdullah, F. Che Pa, H. Mohamad, W.M.A.W. Ibrahim, J. Chaiprapa, Influences of SiO2, Al2O3, CaO and MgO in phase transformation of sintered kaolin-ground granulated blast furnace slag geopolymer, J. Mater. Res. Technol. 9 (2020) 14922–14932, https://doi.org/10.1016/j.jmrt.2020.10.045.
[43] A. Kumar, P. Lingfa, Sodium bentonite and kaolin clays: comparative study on their FT-IR, XRF, and XRD, Mater. Today Proc. 22 (2020) 737–742, https://doi.org/10.1016/j.matpr.2019.10.037.
[44] A. Mebrek, H. Rezzag, S. Benayache, A. Azzi, Y. Taïbi, S. Ladjama, N. Touati, A. Grid, S. Bouchoucha, Effect of chamotte on the structural and microstructural characteristics of mullite elaborated via reaction sintering of Algerian kaolin, J. Mater. Res. Technol. 8 (2019) 4010–4018, https://doi.org/10.1016/j.jmrt.2019.07.009.
[45] A. Yaya, E.K. Tiburu, M.E. Vickers, J.K. Efavi, B. Onwona-Agyeman, K.M. Knowles, Characterisation and identification of local kaolin clay from Ghana: a potential material for electroporcelain insulator fabrication, Appl. Clay Sci. 150 (2017) 125–130, https://doi.org/10.1016/j.clay.2017.09.015.
[46] J.B. Kirabira, S. Jonsson, J.K. Byaruhanga, Beneficiation and evaluation of Mutaka kaolin, Second Int. Conf. Advaces Eng. Technol. (2011) 169–175.
[47] M. El Alouani, S. Alehyen, M. El Achouri, M. Taibi, Preparation, characterization, and application of metakaolin-based geopolymer for removal of methylene blue from aqueous solution, J. Chem. 2019 (2019) 1–14, https://doi.org/10.1155/2019/4212901.
[48] A. Behnamfard, K. Chegni, R. Alaei, F. Veglio, The effect of thermal and acid treatment of kaolin on its ability for cyanide removal from aqueous solutions, Environ. Earth Sci. 78 (2019) 408, https://doi.org/10.1007/s12665-019-8408-8.
[49] H. Douiri, S. Louati, S. Baklouti, M. Arous, Z. Fakhfakh, Structural and dielectric comparative studies of geopolymers prepared with metakaolin and Tunisian natural clay, Appl. Clay Sci. 139 (2017) 40–44, https://doi.org/10.1016/j.clay.2017.01.018.
[50] N. Worasith, B.A. Goodman, N. Jeyashoke, P. Thiravetyan, Decolorization of rice bran oil using modified kaolin, J. Am. Oil Chem. Soc. 88 (2011) 2005–2014, https://doi.org/10.1007/s11746-011-1872-2.

[51] M. Ivanović, L. Kljajević, M. Nenadović, N. Bundaleski, I. Vukanac, B. Todorović, S. Nenadović, Physicochemical and radiological characterization of kaolin and its polymerization products, Mater. Construcción 68 (2018) e155, https://doi.org/10.3989/mc.2018.00517.
[52] F. Bouzerara, A. Harabi, S. Condom, Porous ceramic membranes prepared from kaolin, Desalin. Water Treat. 12 (2009) 415–419, https://doi.org/10.5004/dwt.2009.1051.
[53] K. Pélissier, D. Thierry, Powder and high-solid coatings as anticorrosive solutions for marine and offshore applications? A Review, Coatings 10 (2020) 916, https://doi.org/10.3390/coatings10100916.
[54] P. Wang, Q. Sun, Y. Zhang, J. Cao, One-step hydrothermal synthesis of zeolite KA from kaolin, Micro & Nano Lett. 14 (2019) 1298–1302, https://doi.org/10.1049/mnl.2019.0190.